The structural safety assessment of a tie-down system on a tension leg platform during hurricane events

Chan K. Yang[1] and M.H. Kim*[2]

[1]Technip, Houston, TX, USA
[2]Department of Civil Engineering, Texas A&M University, College Station, TX, USA
(Received November 4, 2011, Revised November 25, 2011, Accepted December 2, 2011)

Abstract.   The performance of a rig tie-down system on a TLP (Tension Leg Platform) is investigated for 10-year, 100-year, and 1000-year hurricane environments. The inertia loading on the derrick is obtained from the three-hour time histories of the platform motions and accelerations, and the dynamic wind forces as well as the time-dependent heel-induced gravitational forces are also applied. Then, the connection loads between the derrick and its substructure as well as the substructure and deck are obtained to assess the safety of the tie-down system. Both linear and nonlinear inertia loads on the derrick are included. The resultant external forces are subsequently used to calculate the loads on the tie-down clamps at every time step with the assumption of rigid derrick. The exact dynamic equations including nonlinear terms are used with all the linear and second-order wave forces considering that some dynamic contributions, such as rotational inertia, centripetal forces, and the nonlinear excitations, have not been accounted for in the conventional engineering practices. From the numerical simulations, it is seen that the contributions of the second-order sum-frequency (or springing) accelerations can be appreciable in certain hurricane conditions. Finally, the maximum reaction loads on the clamps are obtained and used to check the possibility of slip, shear, and tensile failure of the tie-down system for any given environment.

Keywords: safety; tie-down system; derrick; wind-inertia-gravity loading; slip-shear-tensile failure; hurricane; second-order sum-frequency wave forces.

1. Introduction

Many offshore platforms have been installed in Gulf of Mexico (GoM) since the offshore oil and gas industry was born. Most of them have been designed for 100-year hurricane as recommended by API (1993). During the two-year span of 2004-2005, however, three successive events of category-5 (1000-yr) hurricanes, Ivan, Katrina, and Rita, occurred and damaged numerous drilling and production platforms along their paths (e.g., Sgouros *et al.* 2005 and Yang *et al.* 2010a). One of the most significant damages of the floating systems involved the shifting or overturning of derricks. Typically, the drilling and work-over rigs are tied down or fastened to the decks by bolt clamps or pneumatic grip. Many failures of the tie-down system during the recent extreme events raised the question whether the current design philosophy or criteria are suitable. This study is motivated by the demands to prevent future due to extreme events (Ward *et al.* 2006, 2010) in the future.

Currently, the structural design of top-side equipment is usually based on the design standards,

---

*Corresponding author, Professor, E-mail: m-kim3@neo.tamu.edu

such as API Spec 4F(API 1995) and API RP 2A(API 1993). The estimation of the design load on the sea fastening device follows the recommendation by API-Spec 4F, in which the inertia and gravity forces are obtained from wave-frequency linear motions and the phase differences among wind, inertia, and gravity forces are ignored assuming that this method will lead to conservative design. However, since the nonlinear force/motion contributions are ignored, the survivability of the structure is not guaranteed and more advanced methods including all the left-over dynamic contributions (such as centripetal forces and rotary inertia loading ignored in the design practices) and nonlinear effects need to be developed.

Yang *et al*. (2010a) analyzed the dynamic loads on the derrick and its sub-structure on a TLP and a Spar for the post-Katrina Hurricane conditions. The paper reported that spars typically experience larger inertia and heel-induced gravity forces than TLPs due to larger rotational motions. Nonlinear wave-force effects were, however, not included in the paper. For instance, the TLP acceleration at the derrick's center of mass is expected to appreciably increase by including second-order sum-frequency wave excitations. To the best knowledge of the authors, the effects of the sum-frequency accelerations on the safety assessment of the rig tie-down system have never been investigated in the open literature.

In particular, a new feature of coupling floating platform dynamics with the dynamic loads on the derrick by a finite element (FE) spring model has been added to the hull-mooring-riser fully coupled dynamic analysis program (e.g., Kim *et al*. 2001, 2005, 2009, Ran *et al*. 1997 and Yang *et al*. 2010b). Using the developed program, the survivability of a bolt-clamp-based tie-down system on a TLP designed for 3000-ft (914 m) water depth is investigated for extreme hurricane events. Typical 10-year, 100-year, and 1000-year return-period winds, waves, and currents are considered as extreme environmental conditions. A diffraction/radiation 3D panel program (Lee *et al*. 1991) is used to calculate the hydrodynamic coefficients (added mass and radiation damping) and the first-order wave-frequency and second-order sum- and difference-frequency wave excitation forces. Due to the stiff tendon system of the TLP, the heave, roll, and pitch natural periods are around 3 seconds and the surge-sway natural periods are about 170 seconds, namely out of the wave-frequency range. Thus, the second-order wave loads at sum and difference frequencies can be important in predicting the high-frequency (springing) vertical-plane motions and low-frequency (slow drift) horizontal-plane motions. In addition to the potential-based wave diffraction forces, the present time-domain simulation method also includes viscous drag forces on respective Morison members at their instantaneous positions up to the instantaneous free-surface position, which leads to another nonlinear effect. The viscous forces are calculated through the modified Morison equation based on relative velocity squared.

In the present analysis, it is assumed that the derrick is rigid and connected to the TLP hull through springs of large stiffness so that it can be applied to a wider range of applications. The connection may fail if the forces acting on the connector exceed the capacity of slip, shear, and tensile failure modes. The capacities are predetermined by the pretension of the bolts, friction coefficients, and the number of bolts at each footing (Salmon *et al*. 1995). In this regard, the safety of the tie-down-system is extensively examined against various pre-set and hurricane conditions.

2. TLP specification

The principal dimensions of the platform are tabulated in Table 1 (Kim *et al*. 2001a). The TLP

Table 1 Principal dimensions of the TLP

Water depth	(m)	914.36
Number of columns		4
Column cross section diameter	(m)	16.46
Column center to center distance	(m)	60.96
Column freeboard	(m)	20.42
Pontoon breadth	(m)	8.23
Pontoon height	(m)	7.31
Height of deck bottom from MWL	(m)	22.86
Deck height	(m)	12.19

consists of four circular columns of 16.46 m (54 ft) outer diameter connected at the keel by rectangular pontoons of 8.23 m (27 ft) width and 7.31 m (24 ft) height. The center to center span is 60.96 m (200 ft). The hull is attached to eight tendons (two tendons at each column). Moreover, one drilling TTR (top-tensioned riser) and seven production TTRs are connected to the hull by hydraulic pneumatic tensioners at 36.60 m (120.08 ft) above the mean water level (MWL). The detailed configurations are shown in Fig. 1, which also shows the location of the TTR slots (P1-P7 for production, D1 for drilling) and the tendon porch.

The in-place draft, 24.38 m (80 ft), is selected as a base case to estimate the hydrostatic and mass properties. The corresponding hull and load condition are shown in Table 2. The total weight is 24,157 MT (53,256 kips), the total tendon pretension at the top (porch) is 7,031 MT (15,500 kips), and the riser total pretension at the top is 1,588 MT (3,500 kips). The vertical center of gravity (COG) is at 8.56 m (28.1 ft) above MWL and the vertical center of buoyancy (COB) is at 15.18 m (49.8 ft) below MWL. The roll and pitch radii of gyration are 33.19 m (108.9 ft) and the yaw radius of gyration is 32.40 m (106.3 ft).

Fig. 1 Configuration of the TLP hull

Table 2 Hull load condition at in-place draft

Draft	(m)	24.38
Total weight	(MT)	24,157
Total tendon pretension at the top	(MT)	7,031
Riser pretension at the top	(MT)	1,588
Displacement	(MT)	32,775
Vertical center of gravity from MWL	(m)	8.56
Vertical center of buoyancy from MWL	(m)	−15.18
Roll radius of gyration	(m)	33.19
Pitch radius of gyration	(m)	33.19
Yaw radius of gyration	(m)	32.40
Wind load coefficient*	(kN/(m/sec)^2)	3.18
Center of pressure from MWL	(m)	38.10

* Wind load coefficient is for *x*- and *y*- direction.

The wind load coefficient in *x*- and *y*- direction is $C_{eff\_X} = C_{eff\_Y} = F_w / V_{10}^2 = 3.184$ kN/(m/sec)^2 = 0.0665 kips/(ft/sec)^2, where F_w is total wind force on the hull exposed to air and V_{10} is the 1-hour averaged wind speed at 10-m above MWL. For 135-degree heading, the wind load coefficient is increased by the factor 1.414 due to the corresponding increase of the projected area compared to 0- and 90-degree headings. The arrangement of tendons and TTRs is shown in Fig. 2 depicting the TTR connections to the deck and the tendon attachments to the porch location.
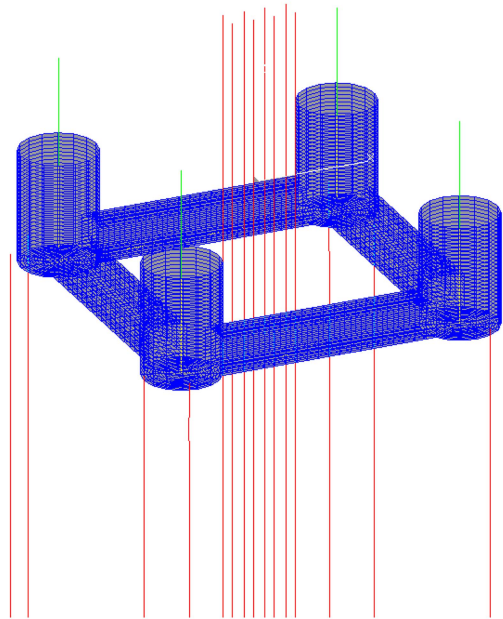
Fig. 2 Arrangement of hull, tendons, and risers

3. Numerical modeling

3.1 Dynamic system

In this section, the motions of multiple rigid bodies subject to general forces are described. The platform, the derrick, and the substructure are treated as separate multiple bodies, each of which has six DOF (degrees of freedom). In general, the N-body system has $6 \times N$ DOFs. The dynamics of N-rigid-body system is derived here assuming that each body is connected through general springs.

The force and moment equilibrium of the i-th body give the equations of motion of the i-th body. The set of equations can be combined into the following form

$$[M^{(i)}]\{\underline{\ddot{y}}^{(i)}\} + \{\underline{N}_v^{(i)}\} = \{\underline{E}_B^{(i)}\} + \{\underline{E}_e^{(i)}\} \tag{1a}$$

where

$$[M^{(i)}] = \begin{bmatrix} [m^{(i)}] & -[m^{(i)} b_g^{(i)\times}] \\ [m^{(i)} b_g^{(i)\times}] & [I^{(i)}] \end{bmatrix} \tag{1b}$$

$$\{\underline{\ddot{y}}^{(i)}\} = \begin{bmatrix} \underline{\ddot{r}}_C^{(i)} \\ \underline{\ddot{\theta}}_{B/N}^{(i)} \end{bmatrix} \tag{1c}$$

$$\{\underline{N}_v^{(i)}\} = \begin{Bmatrix} -[\underline{\dot{\theta}}_{B/N}^{(i)\times}][m^{(i)} \underline{b}_g^{(i)\times}]\{\underline{\dot{\theta}}_{B/N}^{(i)}\} \\ [\underline{\dot{\theta}}_{B/N}^{(i)\times}] \quad [I^{(i)}] \quad \{\underline{\dot{\theta}}_{B/N}^{(i)}\} \end{Bmatrix} \tag{1d}$$

In the above equations, upper-dot means time derivative, $\{\underline{E}_B^{(i)}\}$ is the body force such as gravity, $\{\underline{E}_e^{(i)}\}$ is the external force on the i-th body, $m^{(i)}$ is body mass, $[m^{(i)}]$ and $[I^{(i)}]$ are the 3×3 matrices for mass and mass moment of inertia of the i-th body, $\underline{r}_C^{(i)}$ is the displacement of the rotational center of the i-th body with respect to the inertia coordinate, $\underline{b}_g^{(i)}$ = body-frame displacement of the center of gravity, $\underline{\dot{\theta}}_{B/N}^{(i)}$ = rotational velocity of the body with respect to the inertia frame. The cross matrix $[\underline{b}_g^{(i)\times}]$ is a skew matrix defined as

$$[\underline{b}_g^{(i)\times}] = \begin{bmatrix} 0 & -b_{g3}^{(i)} & b_{g2}^{(i)} \\ b_{g3}^{(i)} & 0 & -b_{g1}^{(i)} \\ -b_{g2}^{(i)} & b_{g1}^{(i)} & 0 \end{bmatrix}$$

and the cross matrix $[\underline{\dot{\theta}}_{B/N}^{(i)\times}]$ is a skew matrix defined as

$$[\underline{\dot{\theta}}_{B/N}^{(i)\times}] = \begin{bmatrix} 0 & -\dot{\theta}_3^{(i)} & \dot{\theta}_2^{(i)} \\ \dot{\theta}_3^{(i)} & 0 & -\dot{\theta}_1^{(i)} \\ -\dot{\theta}_2^{(i)} & \dot{\theta}_1^{(i)} & 0 \end{bmatrix}$$

The nonlinear inertia term $\{\underline{N}_v^{(i)}\}$ becomes negligible when rotational motions are small.

However, when rotational motions are large, it should be retained.

The external forces represent environmental loads, such as wave, wind, and current forces. In case of floating platforms

$$\{\underline{F}_e\} = -[M^a(\infty)]\{\underline{\ddot{y}}\} + \{\underline{F}_R(\underline{\dot{y}},t)\} - [K + K_C(\underline{y},t)]\{\underline{y}\}$$
$$+ \{\underline{F}_{WE}(t)\} + \{\underline{F}_{Wind}(t)\} + \{\underline{F}_{Mor}(\underline{\dot{y}},t)\} + \{\underline{F}_C(\underline{y},\underline{\dot{y}},t)\} \tag{2a}$$

where

$[M^a(\infty)]$: added mass at infinite frequency,

$\underline{F}_R(\underline{\dot{y}},t) = -\int^t R(t-\tau)\underline{\dot{y}}d\tau$: wave radiation damping force including memory effect,

$R(t) = \dfrac{2}{\pi}\int_0^\infty C(\omega)\cos\omega t \, d\omega$: Retardation function from radiation-damping coefficient($C(\omega)$),

$[K]$: system stiffness matrix (hydrostatic),

$[K_C]$: nonlinear implicit time and motion dependent stiffness matrix,

$\underline{F}_C(y,\dot{y},t)$: motion and time dependent connection forces

$\underline{F}_{WE}(t) = \underline{F}_{WE}^{(1)}(t) + \underline{F}_{WE}^{(2)}(t)$: potential-based wave exciting forces of the first and the second order,

$\underline{F}_{Wind}(t)$: dynamic wind loading,

$\underline{F}_{Mor}(y,\dot{y},t)$: force on the Morison members whose primary contribution is viscous loading (current loading is included here),

The index "*i*" is omitted in the equation for convenience. In case of top-side structures on the deck, such as derrick and the substructure, the added mass, hydrostatic, radiation damping, wave excitation force, and Morison force terms disappear and the equation of motion is simplified to

$$\{\underline{F}_e\} = -[K_C(\underline{y},t)] + F_{Wind}(t) + F_C(\underline{y},\underline{\dot{y}},t) \tag{2b}$$

The nonlinear stiffness K_C and the nonlinear connection forces $F_C(\underline{y},\underline{\dot{y}},t)$ between bodies are mostly from the nonlinear FE model of mooring/tendon and risers for offshore platforms or the nonlinear/linear spring between bodies for top-side structures (Yang 2009).

In the present study, the linear spring model of large stiffness is applied at the footings of the derrick and its substructure to calculate the reaction loads at the respective locations. The nonlinear spring model allowing finite displacements can be used in the case of float-over installation from a transportation barge to installation barges.

3.2 Hydrodynamic modeling

The added mass and radiation damping coefficients, first-order wave-frequency wave excitation forces, and second-order sum- and difference-frequency wave forces are calculated by the second-order diffraction/radiation panel program (Lee *et al*. 1991). Since the natural frequencies of the vertical-plane motions of a TLP are higher than typical incident-wave frequencies, the inclusion of the second-order sum-frequency (or springing) wave excitations is very important (Kim and Yue 1990). Similarly, the inclusion of the second-order difference-frequency (or slow-drift) wave excitations is important for horizontal-plane motions. The stiffness due to tendons and the TTRs is considered in the frequency-domain for the second-order wave force calculations that depend on
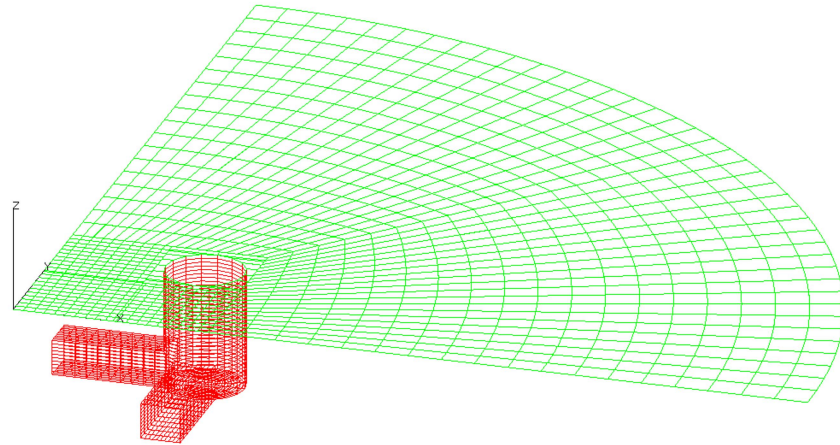
Fig. 3 Panels on the hull and free surface for the 2nd-order hydrodynamic computation

first-order motions (Kim and Yue 1990). All the hydrodynamic coefficients are calculated in the frequency domain, and the corresponding forces are converted to the time domain by using two-term Volterra series expansion (Kim and Yue 1991). The frequency-dependent radiation damping was included in the form of convolution integral in the time-domain simulation. The origin of the body-fixed coordinate system is located on the MWL (mean water level) at the center of the hull. The *z*-axis is positive upward. In Fig. 3, the panel configuration for the second-order diffraction/radiation computation is shown. In the second-order computation, the near-field free surface inside the truncation circle also needs to be discretised. One quadrant of the TLP hull surface is discretized by 1420 panels and that of the inner free surface is discretized by 1070 panels. The truncation radius used here is 165 m (540 ft). Outside the truncation radius, analytic integrations are used, as described in Lee *et al*. (1991).

3.3 Tendon and riser modeling

The tendons and risers are modeled by a high-order FE method based on the slender rod theory (Garret 1982). Eight tendons and eight TTRs are modeled, as shown in Fig. 2. After checking the convergence, each tendon or riser is discretized by 25 higher-order FEs(finite elements) which are quadratic in displacement and cubic in tension. The eight TTRs consist of one drilling riser of 205.9MT tension and seven production risers of 104.3MT tension. The tensioner stiffness of the TTR is assumed to be 364.87 kN/m (25 kips/ft). The hydrodynamic loads on the elements are calculated by the Morison equation. The tendons and risers are connected to the sea bed with linear springs of large-stiffness, which is equivalent to hinged joint. The tendons are connected to the hull by the same linear springs, while the TTRs are coupled with it by a flexible pneumatic tensioner. The numerical model of the tensioner is given, for example, in Yang *et al*. (2010c). The relation between the nominal tension (*T*) and the stroke (*z*) of the tensioner is given by the following nonlinear relation

$$T = \frac{T_0}{(1 + z/z_0)^n} \tag{3}$$

where z_0 = nominal length of the associated accumulator, T_0 = Initial top tension at stroke z = 0, and n = gas constant.

The coulomb friction force (f_f) between the tensioner piston and the cylinder is modeled following Andrighetto *et al*. (2005)

$$f_f = \mu_T T \text{sign}(-\dot{z}) \tag{4}$$

where μ_T = dynamic friction factor of the tensioner, $\dot{z}$ = time derivative of the stroke. The time varying friction force changes its direction depending on the sign of the relative velocity. The dynamic friction factor m_T is typically set in the range of 0.02-0.05. In the present case, a typically recommended value of 0.025 was used.

4. Environmental criteria

The water depth is 914 m (3000 ft). 10-year, 100-year, and 1000-year hurricanes are selected as example storm conditions. Table 3 shows the corresponding wave, wind, and current characteristics of each environmental condition. JONSWAP spectra are used with the input significant wave heights, peak periods, and peakedness parameters (γ) to represent the respective irregular uni-directional waves. It is confirmed that the regenerated wave spectra derived from the generated time histories coincide with the input spectra. The time varying wind speed is generated by the similar method by using the API wind spectrum. The current velocities decay with depth, as shown in Table 3. The wind-wave-current are assumed to be collinear with the incident angle of 135 degrees. The currents are assumed to be steady and applied on the submerged part of the platform.

Table 3 Environmental criteria

Return period	10 year		100 year		Ivan (1000 year)	
Hs (m)	7.59		12.19		15.57	
Tp (sec)	11.9		14		15.6	
Gamma (γ)	2.4		2.4		3	
Wind speed (knot)	50.9		81.3		87.9	
Current profile	Depth (m)	Speed (m/s)	Depth (m)	Speed (m/s)	Depth (m)	Speed (m/s)
	0.00	0.79	0.00	1.50	0.00	2.50
	29.99	0.60	29.99	1.15	5.00	2.50
	60.01	0.29	60.01	0.56	24.99	1.19
	90.00	0.10	90.00	0.10	50.02	1.12
	914.36	0.10	914.36	0.10	80.49	0.74
					100.00	0.31
					150.02	0.29
					300.00	0.27
					914.36	0.00

Table 4 Natural periods and damping factors

	Tn (sec)	X Critical damping
Surge	169.98	11.15%
Sway	169.98	11.98%
Heave	3.38	4.77%
Roll	2.96	4.70%
Pitch	3.02	4.01%
Yaw	124.58	8.90%

5. Numerical results and discussions

A series of numerical free-decay tests are carried out to measure the natural periods and the damping ratios for the TLP's 6-DOF motions. The results are summarized in Table 4. The heave natural period is 3.35 seconds and the roll/pitch natural periods are 3.01/2.96 seconds. The surge and sway natural periods are around 170 seconds with the damping ratio of 11-12%.

A definition sketch of the free-body diagram of the top-structure on the platform with the applied forces is shown in Fig. 4. The time-varying gravity, inertia, and wind loads are included as external loading on the derrick. The gravity/inertia forces are acting at center of gravity, while the wind force is acting at the center of pressure.

The detailed configuration of the derrick and substructure is shown in Fig. 5. The derrick is
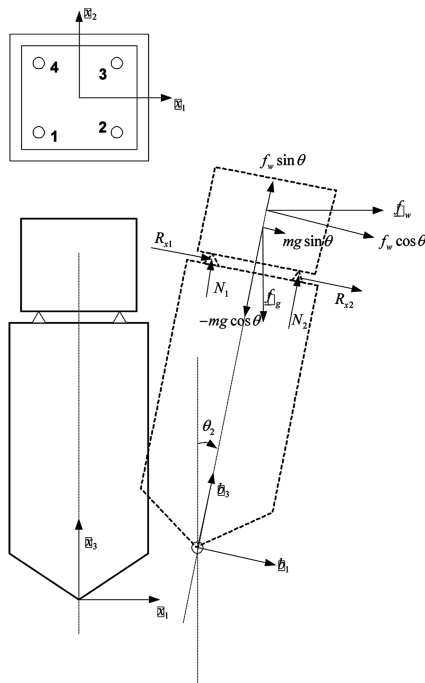
Fig. 4 Definition sketch of the coordinate system and free body diagram of the derrick
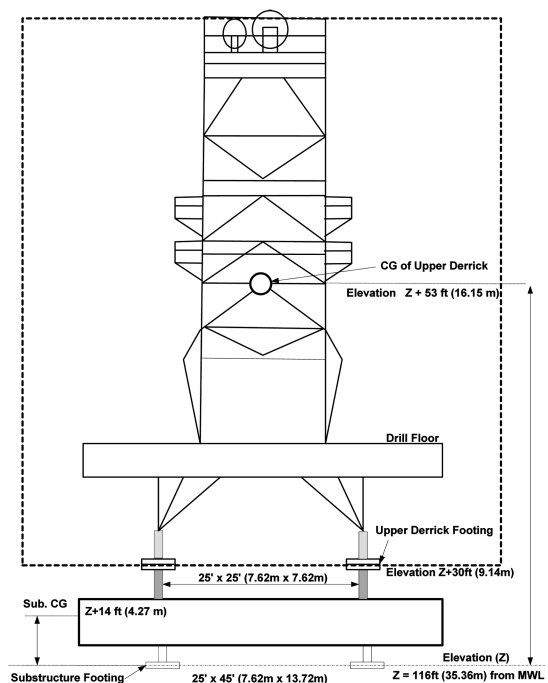
Fig. 5 Configuration of the derrick and the substructure

Table 5 Specifications of Upper-Derrick and sub-structure

	Upper derrick	Substructure	Total
Weight (MT)	249.48	680.40	929.87
Projected area* (m^2)	273.11	46.45	319.56
Center of pressure from MWL (m)	61.26	39.62	57.91
Center of gravity from MWL (m)	51.51	39.62	42.82
Height coefficient(C_h)	1.37	1.19	1.24
Shape coefficient(C_s)	1.25	1.25	1.25
Radius of gyration around CG (m)	4.57/4.57/3.05	4.57/4.57/3.05	6.10/6.10/3.05

* The projected area is for *x*- and *y*- direction, and 1.414 times of it is used for 135 degree heading.

connected to the deck through the substructure. The derrick footings connect the derrick to the substructure, and the substructure footings connect the substructure to the deck. The substructure footing is 33.36 m (116 ft) from the mean water level and the derrick footing is positioned 9.14 m (30 ft) above the substructure footing. The derrick/substructure particulars are given in Table 5. The derrick and the substructure are assumed to be positioned at the center of the deck. The derrick projected area in *x*- or *y*-direction is 136.6 m^2 (1470 ft^2). It is assumed that the front part of derrick does not shade the area downstream. Thus, twice the value 273.1 m^2 (= 2940 ft^2) is used for the wind-loading calculation.

A plan view of the footing layout is shown in Fig. 6. The derrick footings are on the rail parallel to the *y*-axis to allow slip only in *y*-direction. The shear force in *x*-direction is resisted by the clamp bolts of the tie-down system. The substructure footings are laid on the deck-rail parallel to *x*-direction to allow slip in that direction. Each footing is designed to have eight bolts to provide sufficient resistance against slip, shear, and tensile loadings, as shown in Fig. 7. With the given
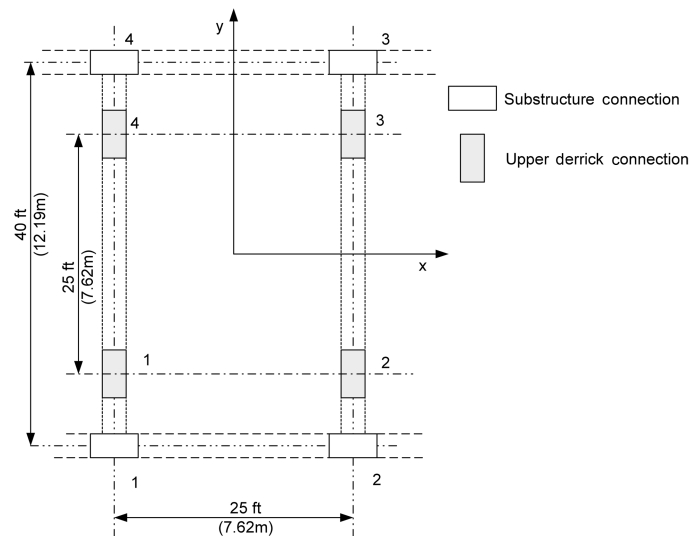

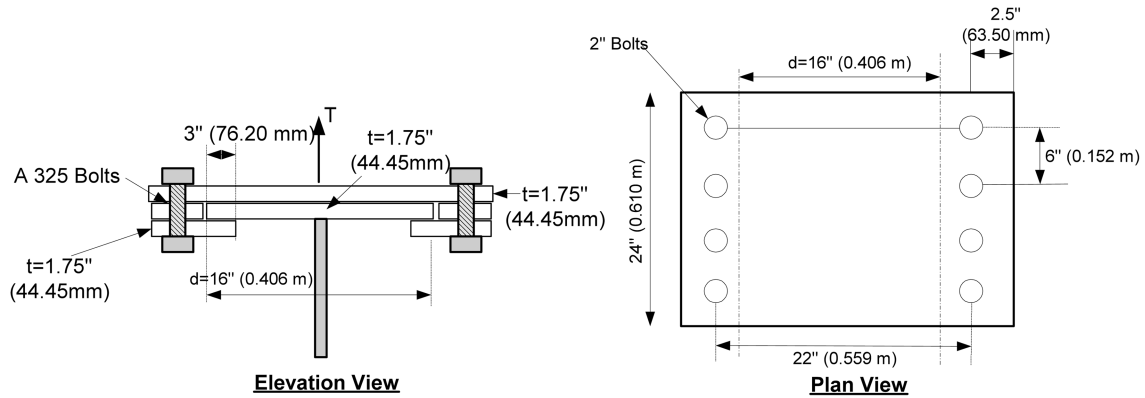Fig. 6 Configuration of the upper derrick and the substructure footings

Fig. 7 A typical connection at derrick base and substructure base

layout of the bolts, the shear force is resisted by 4 bolts, while the tensile force is resisted by 8 bolts per footing. In the present example, 1-1/2-inch bolts are used to tie down the structures and the corresponding shear and the tensile capacities for each bolt are estimated based on its material property. The slip is to be prevented by the friction force primarily caused by the bolt tension. The friction force is also dependent on the friction factor between the two contacting materials.

The slip and tensile capacity of the footings are closely related to the bolt pretension. Four values of pretension are considered for the present study corresponding to $T_0 = 334$, 611, 667, and 1,001 kN, among which $T_0 = 611$ kN ($= 55\%$ of tensile breaking loading per bolt) is the recommended value by AISC (American Institute of Steel Construction). The higher the pretension is, the higher the slip capacity becomes with the greater friction force. However, the higher pretension results in lower tensile capacity. So, there is a trade-off between slip and tensile capacity. The slip capacity (μN, $N = normal\ force$) also varies depending on the friction factor μ. The friction factor between two steel surfaces can be as low as $\mu = 0.1$ in a very wet condition but can reach 0.5 when they are dry. For the Hurricane condition, the tie-down system is exposed to water or humidity and the friction factor becomes close to 0.1. Once it starts to slip, the friction factor becomes even smaller, and the system cannot avoid the successive slip as long as similar loadings are there.

The total wind forces are calculated based on the projected area, shape coefficient, and height coefficient as follows.

$$F_{wind} = 1/2\rho_{air}A_{project}C_hC_sV^2_{10m}(t) \tag{5}$$

where $V_{10m}(t)$ is the instantaneous wind velocity at 10m above mean water level and ρ_{air} is the air density. C_h is the height coefficient to adjust the wind velocity from 10 m to the wind pressure center, and C_s is the shape coefficient similar to the drag coefficient.

5.1 Derrick motion and acceleration

Three-hour time-domain simulations are carried out for three different hurricane conditions as described in the previous sections. The maximum offset of the TLP for 100-year hurricane is about 12.6% of WD (water depth). For the same condition, the maximum heel angle is 0.5 degrees and the corresponding maximum horizontal and vertical accelerations (excluding the heel-angle effect) at

the hull center of gravity are 15% and 2% of g (gravitational acceleration). The accelerations cause inertia loading on deck structures. The API 4F recommends to calculate the maximum horizontal and vertical acceleration amplitudes, $a_{x\max}$ and $a_{z\max}$, respectively, as follows

$$a_{x\max} = \omega_p^2(x + r\theta)_{\max} + g\sin\theta_{\max} \tag{6}$$

$$a_{z\max} = \omega_p^2 z_{max} \tag{7}$$

Where $\theta_{\max}$ = maximum pitch, r = distance from structure CG to the coordinate origin, g = gravitational acceleration, $z_{\max}$ = maximum heave, and ω_P = peak wave frequency (rad/s). The force caused by the second term in the right-hand side of (6) is called heel-induced gravitational force.

Table 6-8 show the maximum x-acceleration and z-acceleration at the derrick C.G. calculated in three different methods. The "API 4F" method is based on the above equation by using linear wave-structure interaction theory, The "Revised" method calculates the low-, wave-, and high-frequency maximum accelerations separately by using the second-order wave-structure interaction theory and adds their maximum amplitudes together to get the total maximum acceleration. The "Coupled Analysis" means that the maximum accelerations are directly read from the 3-hour time-domain simulations. For comparison, the relative magnitudes of the low-, wave-, and high-frequency rms accelerations are also given in the same table. It is seen that the contributions of the second-order sum-frequency heave and pitch accelerations are appreciable compared to the first-order wave-frequency heave and pitch accelerations.

Table 6 Comparison of accelerations (10-yr hurricane)

10 year Hurricane Tp = 11.9 (sec)			Low freq	Wave freq	High freq	Total
Motion @ Hull CG	Surge	STD (m)	3.363	0.925	0.028	
		Tz (sec)	161.2	11.6	4.8	
	Heave	STD (m)	0.098	0.038	0.004	
		Tz (sec)	159.9	11.6	4.0	
	Pitch	STD (deg)	0.005	0.048	0.012	
		Tz (sec)	95.2	10.1	3.8	
Acceleration @ Derrick CG	Horizontal	STD (m)	0.008	0.257	0.077	
		Tz (sec)	60.6	10.6	4.3	
	Vertical	STD (m)	0.001	0.013	0.013	
		Tz (sec)	57.6	9.2	3.2	
3 hour Max. Horizontal Acceleration	API 4F	(m/sec²)	Tp = 11.9 sec [1)			1.020
	Revised	(m/sec²)	0.018	1.074	0.257	1.105
	Coupled	(m/sec²)	Direct coupled analysis			1.122
3 hour Max. Vertical Acceleration	API 4F	(m/sec²)	Tp = 11.9 sec			0.039
	Revised	(m/sec²)	0.002	0.050	0.051	0.072
	Coupled	(m/sec²)	Direct coupled analysis			0.081

Table 7 Comparison of accelerations (100-yr hurricane)

100 year Hurricane Tp = 14 (sec)			Low freq	Wave freq	High freq	Total
Motion @ Hull CG	Surge	STD (m)	4.405	1.959	0.037	
		Tz (sec)	131.0	13.6	4.9	
	Heave	STD (m)	0.288	0.138	0.013	
		Tz (sec)	130.2	13.8	4.2	
	Pitch	STD (deg)	0.012	0.066	0.019	
		Tz (sec)	84.3	10.7	3.7	
Acceleration @ Derrick CG	Horizontal	STD (m)	0.016	0.422	0.114	
		Tz (sec)	51.7	11.5	3.7	
	Vertical	STD (m)	0.006	0.035	0.046	
		Tz (sec)	51.2	11.2	3.5	
3 hour Max. Horizontal Acceleration	API 4F	(m/sec^2)	Tp = 14.0 sec[1]			1.518
	Revised	(m/sec^2)	0.037	1.611	0.349	1.649
	Coupled	(m/sec^2)	Direct coupled analysis			1.733
3 hour Max. Vertical Acceleration	API 4F	(m/sec^2)	Tp = 14.0 sec			0.101
	Revised	(m/sec^2)	0.018	0.131	0.186	0.228
	Coupled	(m/sec^2)	Direct coupled analysis			0.237

Table 8 Comparison of accelerations (1000-yr hurricane)

1000 year Hurricane Tp = 15.6 (sec)			Low freq	Wave freq	High freq	Total
Motion @ Hull CG	Surge	STD (m)	4.742	2.922	0.039	
		Tz (sec)	124.0	15.0	4.9	
	Heave	STD (m)	0.408	0.259	0.015	
		Tz (sec)	123.4	15.2	4.2	
	Pitch	STD (deg)	0.017	0.074	0.023	
		Tz (sec)	82.8	11.3	3.6	
Acceleration @ Derrick CG	Horizontal	STD (m)	0.021	0.525	0.129	
		Tz (sec)	50.9	13.1	4.1	
	Vertical	STD (m)	0.005	0.051	0.050	
		Tz (sec)	49.2	12.3	3.5	
3 hour Max. Horizontal Acceleration	API 4F	(m/sec^2)	Tp = 15.6 sec[1]			1.793
	Revised	(m/sec^2)	0.045	1.943	0.387	1.982
	Coupled	(m/sec^2)	Direct coupled analysis			2.050
3 hour Max. Vertical Acceleration	API 4F	(m/sec^2)	Tp = 15.6 sec			0.152
	Revised	(m/sec^2)	0.016	0.187	0.202	0.276
	Coupled	(m/sec^2)	Direct coupled analysis			0.273

To see the relevant physics more clearly, the motion and acceleration spectra of heave and pitch are plotted in Figs. 8 and 9 for three different hurricane conditions. The corresponding statistics results are summarized in Table 6-8. In case of heave spectra, there exist significant low-frequency components due to set-down effects driven by slowly-varying surge-sway motions. However, the corresponding low-frequency accelerations are negligible. Both heave- and pitch-acceleration spectra show peaks at the wave frequency, the springing frequency (sum frequency), and the natural frequency of each mode. The amplitude of motion at the natural period is small but the corresponding acceleration is significant due to its high frequency characteristics. The heave and pitch acceleration spectra are not narrow banded but multi-peaked, so the linear wave-structure interaction theory alone (like the API-4F recommendation) may appreciably under-predict the total vertical accelerations. In this regard, the "Revised" formula better represents the actual physics and gives closer values to those from the direct time-domain simulations including second-order wave-structure interaction effects. The relative importance of high-frequency accelerations compared to wave-frequency ones is more pronounced in heave than in surge, and in 10-yr case than in the other cases. The ratios of the high-frequency STD (standard deviation) accelerations to the wave-frequency STD accelerations at the derrick C.G., for example, are 30% (10-yr), 27% (100-yr), 24% (1000-yr) for the horizontal direction and 100% (10-yr), 131% (100-yr), 98% (1000-yr) for the vertical direction. The majority of the high-frequency excitations are caused by the second-order sum-frequency wave loading from potential theory. There is also a partial contribution from the viscous wave loading.
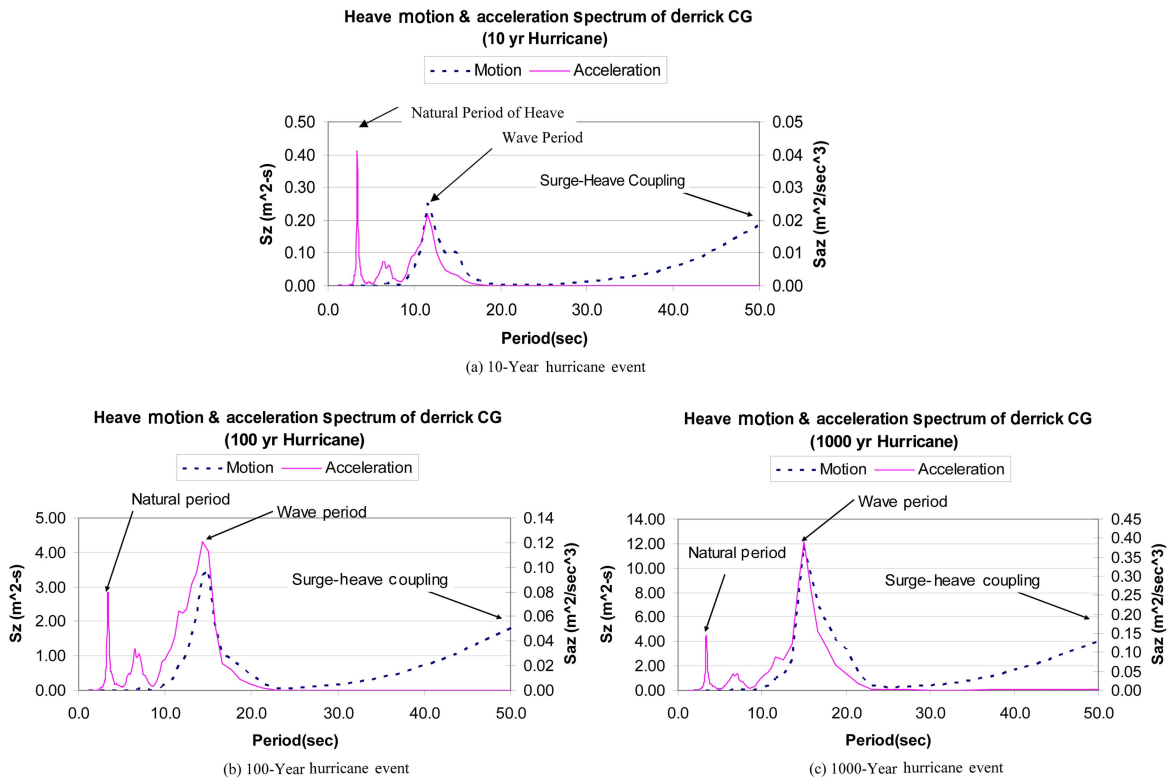

(a) 10-Year hurricane event

(b) 100-Year hurricane event

(c) 1000-Year hurricane event

Fig. 8 Heave motion and acceleration power spectra

Pitch motion & acceleration Spectrum of derrick CG (10 yr Hurricane)

(a) 10-Year hurricane event

Pitch motion & acceleration Spectrum of derrick CG (100 yr Hurricane)

(b) 100-Year hurricane event

Pitch motion & acceleration Spectrum of derrick CG (1000 yr Hurricane)
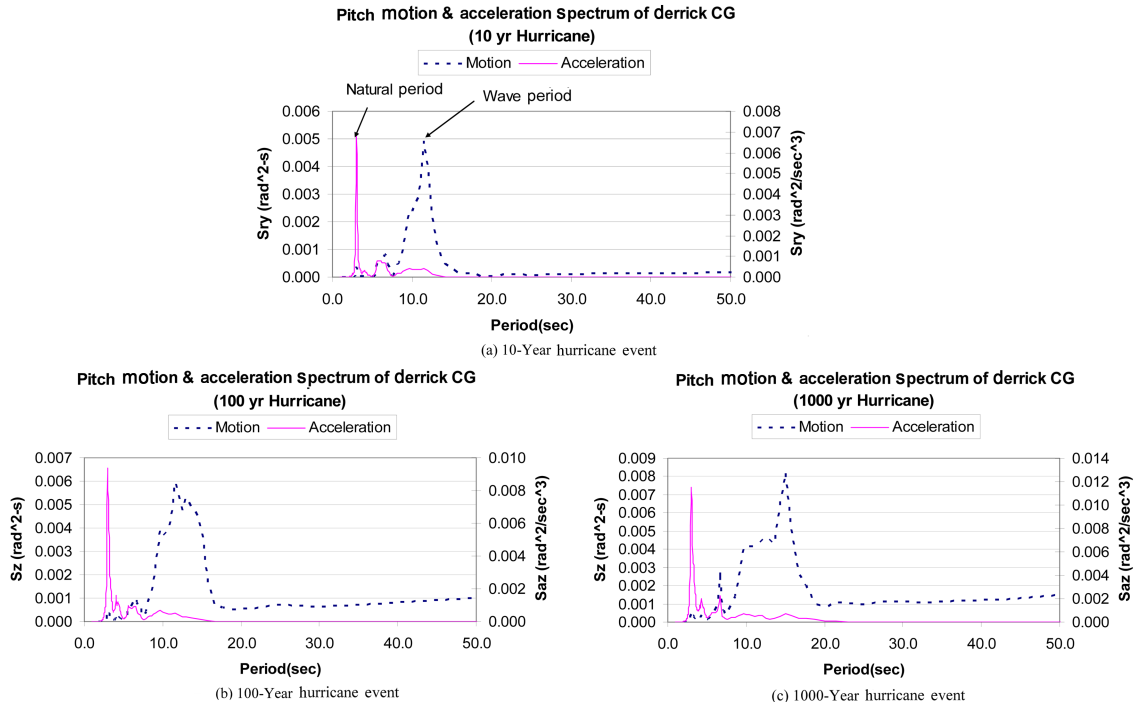
(c) 1000-Year hurricane event

Fig. 9 Pitch motion and acceleration power spectra

5.2 Dynamic forces on derrick and substructure

Fig. 10 shows the time histories of the constituent external horizontal forces (inertia, gravity, and wind loading) and the total force acting on the upper derrick for 100-year hurricane condition. The wind force is greater than twice the inertia loading and the gravity component is negligible due to small heel angles. The maximum (= 963.7 kN) of the total force is smaller than the sum of each maxima (= 1100 kN) due to phase cancellation. In Fig. 11, the maxima of the individual *x*-force components and the total *x*-force are plotted for three different hurricane conditions. When sub-structure is also included, the inertia loading becomes comparable in magnitude against wind loading due to the significant increase of total mass. Fig. 12 plots the corresponding results for the overturning moments with respect to the respective footings. In case of 100-yr hurricane, the total forces on the derrick and substructure are about 23% less than the summation of each maximum. In case of the overturning moment with respect to the substructure footing, the difference is reduced to 13%. In this regard, the phase difference between the force components should be taken into account to avoid too much conservatism on top of the other design margins.

5.3 Reaction forces on footings and safety factor

The reaction forces are calculated by putting the springs at the footing locations. The time histories of the reaction forces at the up-wave derrick footing (#2) in *x*-, *y*- and *z*- directions are plotted in Fig. 13 for 100-year hurricane condition (135-degree heading). F_x causes shear force and F_z causes slip force against the tie-down system. In case of F_z, minus sign means up-lifting force
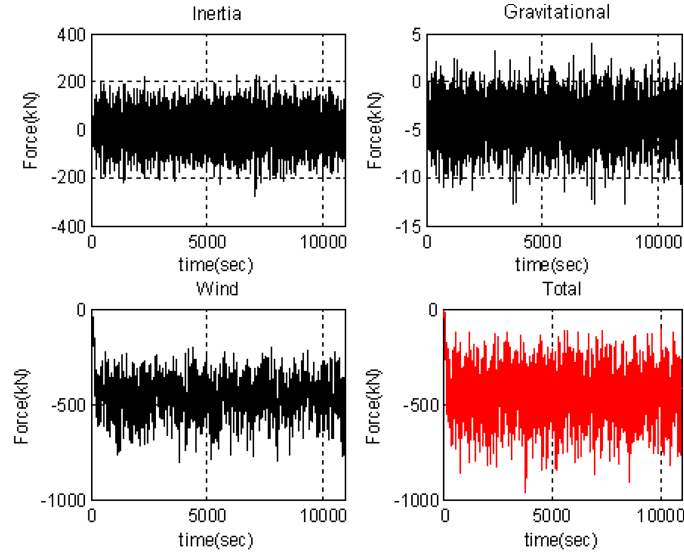
Fig. 10 Inertia, gravitational, and wind forces in *x*-direction acting on the upper derrick for 100-year hurricane condition

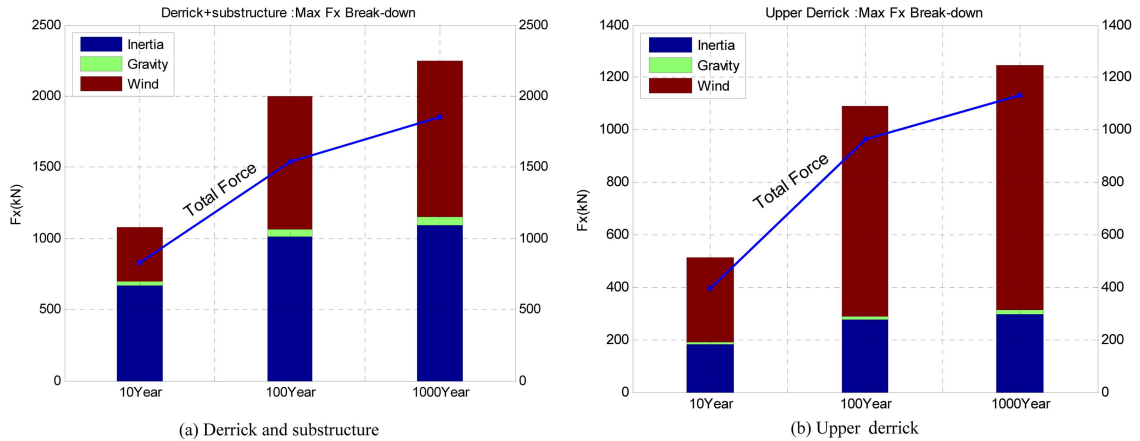(a) Derrick and substructure

(b) Upper derrick

Fig. 11 Constituent and total *x*-directional forces

and it can cause additional tensile force on clamp bolts. The up-lifting force is mainly caused by the overturning moment on the derrick by external loadings. When there is no external load, F_z is positive and equal to one quarter of its weight.

Fig. 14 illustrates how the bolt tension is varying due to the external force when the pre-load T_0 is applied. The bolt system does not feel the entire external load up to some point. In most cases, the majority of this additional load is absorbed by the clamped joint members because the clamp joint is usually much stiffer than the bolts. At some point, however, the external load can be great enough that the clamp load on the joint is completely unloaded (Collins 2002). Any additional load from this point will be entirely additive to the existing bolt tension. The balance between the external loads acting on the bolts and the clamp joint are generally displayed on a graph in Fig. 15. The bolt diameter is 2 inch(50.8 mm), and the thickness of the clamped material(L_m) is 3×7.5 inch

(a) Derrick and substructure   (b) Upper Derrick
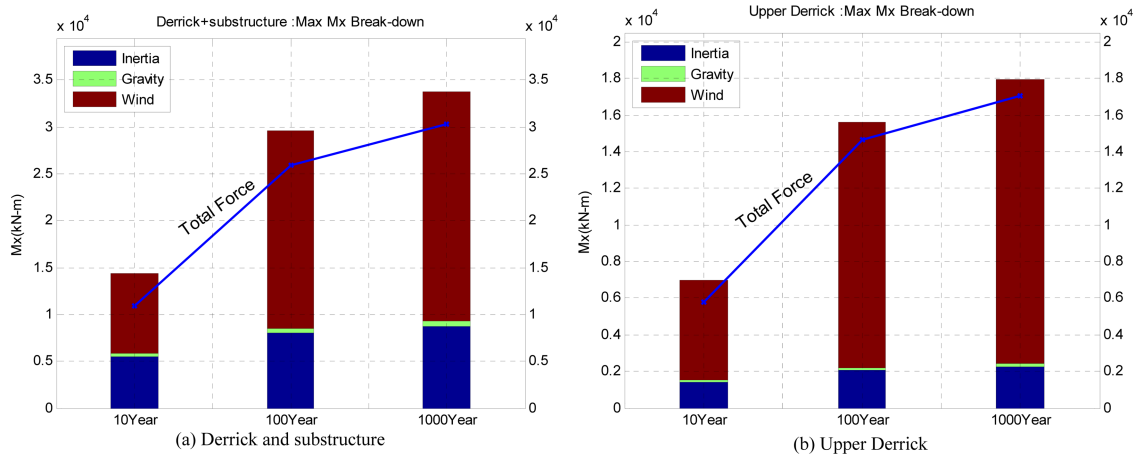
Fig. 12 Constituent and total *x*-directional overturning moments
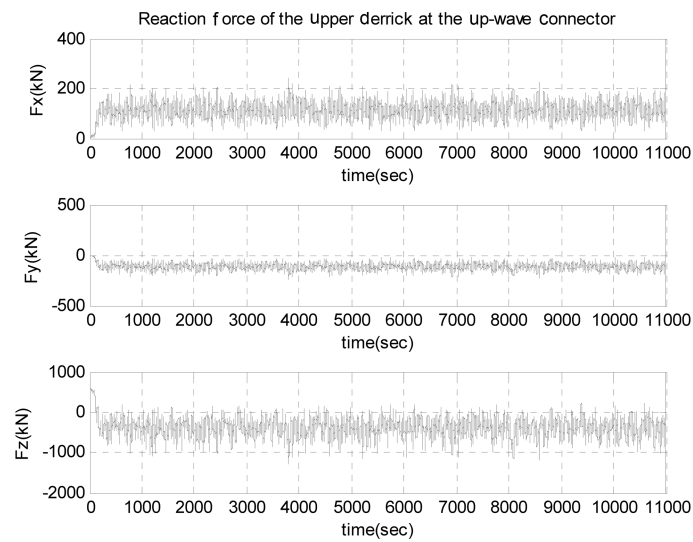
Fig. 13 Reaction forces at the up-wave upper-derrick footings for 100-year hurricane condition

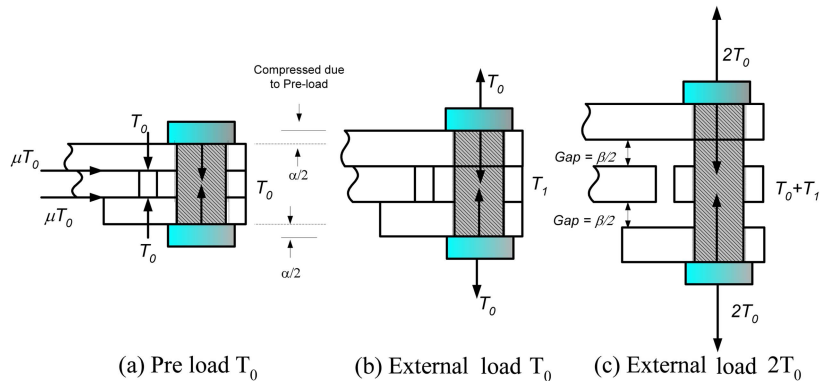(a) Pre load T_0 (b) External load T_0 (c) External load $2T_0$

Fig. 14 Definition sketches of the clamp system with bolt with pre-tensioned by T_0
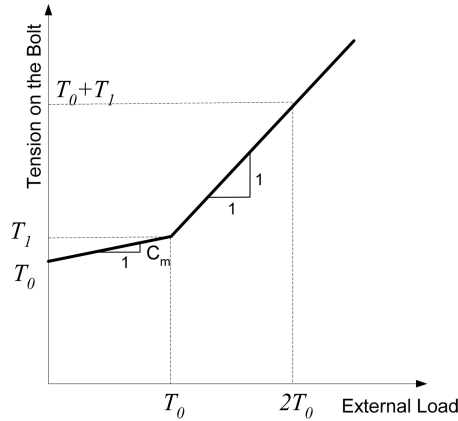
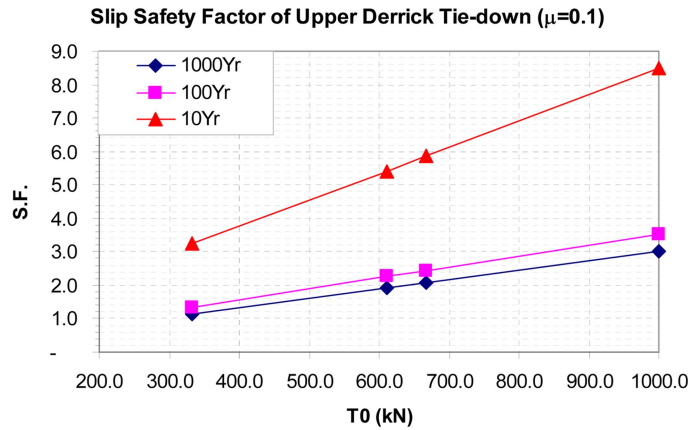Fig. 15 Bolt tension varying due to the external load variation

Fig. 16 Slip safety factor of upper derrick tie-down

(133 mm). Then, the bolt stiffness is calculated to be $k_b = AE/L_m = 3.2 \times 10^9$ N/m, where A is the bolt cross sectional area and E is the Young's modulus (= 210 GPa). The stiffness of the clamped material is $k_m = 13.0 \times 10^9$, and the joint stiffness factor $C_m = k_b/(k_b + k_m) = 0.2$ for this case. In Fig. 15, the slope of the bolt tension to the external load before the joint is fully unloaded is C_m. It becomes 1 after it is fully loaded. The typical joint stiffness factor varies from 0.25 to 0.2. With $C_m = 0.2$, it follows that only 0.2 of the applied load is taken by the bolt.

Figs. 16 and 17 present the slip safety factors(= slip capacity/slip force) of the upper-derrick and sub-structure footing for the worst case scenario i.e., very wet condition with $\mu = 0.1$. The slip capacity is equal to the friction force (= μN, where N is the total normal force caused by bolt pretension and derrick weight). The normal force can be decreased at the weather-side footing due to up-lifting force but it can be compensated at the lee-side footing by the increased compression force. The slip safety factor is highly dependent on the applied pre-tension of the bolts (T_0), and thus they are plotted against four values of T_0. The safety factor below 1 means failure. The slip safety factors of the sub-structure are smaller than those of upper derrick due to the increase of inertia-loading component. The safety factors become less than one at the substructure footing with the lowest pre-tension ($T_0 = 333.6$ kN) and environments equal to or harsher than 100-year
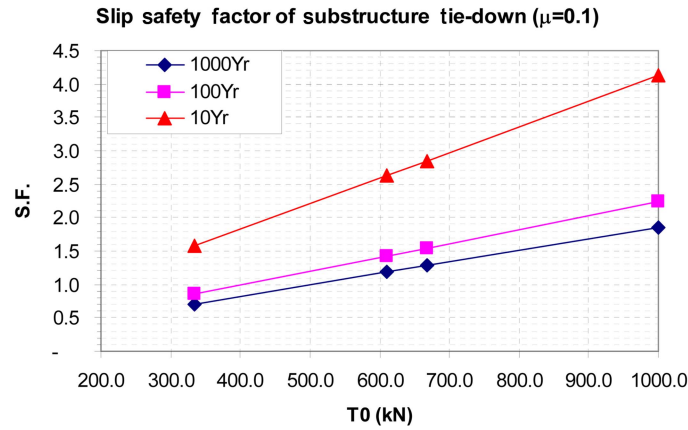
Slip safety factor of substructure tie-down (μ=0.1)

Fig. 17 Slip safety factor of sub-structure tie-down

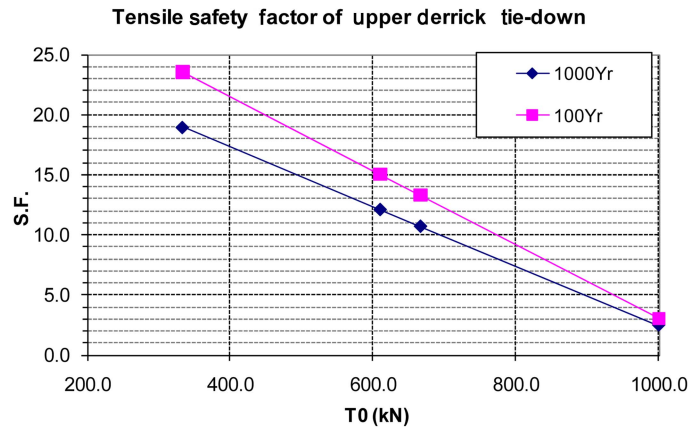**Tensile safety factor of upper derrick tie-down**

Fig. 18 Tensile safety factor of upper derrick tie-down with respect to the initial tension (T_0)

hurricane.

Finally, Fig. 18 plots the tensile safety factors at the upper-derrick up-wave footing against various pre-tensions and hurricane conditions. It is already pointed out that the tensile capacity decreases with increasing pretension, which is opposite to the trend of slip capacity. Therefore, there is a trade-off between slip and tensile capacity. However, the external loads are all below the pre-tension, and only 20% of the external loads are transferred to the bolt as extra tension. It is seen that the tensile safety factor becomes 2.5 in the worst case of the highest bolt pretension $T_0 = 1000.8$ kN and 1000-yr hurricane. In other words, the present tie-down system is safe against bolt-tensile failure up to the given highest bolt-pretension condition.

6. Conclusions

A time-domain-simulation method to assess the performance of the tie-down system on a floating production platform including nonlinear wave effects is developed and applied to a 3000-ft TLP with three different (10-yr, 100-yr and 1000-yr) hurricane conditions. The possibility of slip or

tensile failure of a typical tie-down system at upper-derrick and substructure footings are checked by using the 3-hour time histories based on the full dynamic equations of the platform, derrick, and substructure.

The global motion of the TLP is first simulated by using a time-domain hull-mooring-riser coupled dynamic analysis program. Then, the platform motion and acceleration time series are fed into the derrick dynamic analysis program to obtain the maximum slip and up-lift forces at the respective footing locations. The results are compared with simpler API-4F methodology, which neglects nonlinear wave forces and platform motions, phase cancellation among external loadings, and the effects of rotational inertia and centrifugal forces. The rotational inertia and centrifugal forces are relatively insignificant in the present example, whereas, the contributions of the second-order sum-frequency wave forces to the total inertia loading become appreciable particularly in the vertical direction and need to be taken into consideration. The phase-cancellation effects among constituent external forces can lead to some conservatism though.

The possibility of slip and tensile failure of the given tie-down system for various hurricane conditions is also checked. It is found that the upper-derrick footing is more vulnerable to tensile failure than the substructure footing and the substructure connection is more vulnerable to slip failure compared to the upper-derrick connection, so different bolt pretensions can be applied to the upper-derrick and sub-structure footings for the best structural integrity. If bolt pretension is too small, slip failure is likely to occur. If bolt pretension is too large, the system is vulnerable to tensile failure. Therefore, maintaining proper middle-range tension especially during the hurricane is important. The pretension recommended by AISC ($T_0 = 609$ kN) keeps the structure within the slip and tensile capacity for all the cases considered.

In conclusion, a new method developed here by using the platform nonlinear-motion time series and exact derrick dynamic equations is recommended as a more reliable methodology to check the possibility of slip and tensile failure of derrick connection during extreme hurricane conditions.

Acknowledgments

References

AISC, Manual of steel construction, allowable stress design, 9th Edition.

Andrighetto, P.L., Valdiero, A.C. and Carlotto, L. (2005), "Study of the friction behavior in industrial pneumatic actuators", *Proceedings of the 18th International Congress of Mechanical Engineering*.

API (1995), Specification for drilling and well servicing structures-API Spec. 4F, 2nd Edition.

API (1993), Recommended practice for planning, designing and constructing fixed offshore platforms-load and resistance factor design.

Collins and Jack A. (2002), *Mechanical design of machine elements and machines*, John Wiley & Sons Inc.

Garret, D.L. (1982), "Dynamic analysis of slender rods", *J. Energy. Resour. Technol.*, **104**(4), 302-307.

Kim, M.H., Tahar, A. and Kim, Y.B. (2001a), "Variability of TLP motion analysis against various design methodologies/parameters", *Proceedings of the 11th ISOPE conference*, Stavanger, Norway.

Kim, M.H. and Zhang, Z. (2009), "Transient effects of tendon disconnection on the survivability of a TLP in moderatestrength hurricane conditions", *Int. J. Naval Architect. Ocean Eng.*, **1**(1), 13-19.

Kim, M.H., Koo, B.J., Mercier, R.M. and Ward, E.G. (2005), "Vessel/mooring/riser coupled dynamic analysis of aturret-moored FPSO compared with OTRC experiment", *Ocean Eng.*, **32**(14-15), 1780-1802,

Kim, M.H., Ran, Z. and Zheng, W.(2001b), "Hull/mooring coupled dynamic analysis of a truss spar in time domain", *Int. J. Offshore Polar*, **11**(1), 42-54.

Kim, M.H. and Yue, D.K. (1991), "Sum- and difference-frequency wave loads on a body in uni-directional Gaussian seas", *J. Ship Res.*, **35**, 127-140.

Kim, M.H. and Yue, D.K.P. (1990), "The complete second-order diffraction solution for an axisymmetric body Part 2. bichromatic incident waves and body motions", *J. Fluid Mech.*, **211**, 557-593.

Lee, C.H., Newman, J.N., Kim, M.H. and Yue, D.K.P. (1991), "The computation of second-order wave loads". *Proceedings of the 10th Offshore Mechanics and Artic Eng. Conference*, Stavanger, Norway.

Ran, Z. and Kim, M.H. (1997), "Nonlinear coupled analysis of a tethered spar in waves", *Int. J. Offshore Polar*, **7**(2), 111-118.

Salmon, C.G. and Johnson, J.E. (1995), Steel structures design and behavior, 4th Edition.

Sgouros, G.E., Pritchett, W.M., Schafer, D.R. and Jones, D.L. (2005), "Shell's experience with hurricane ivan", *Proceedings of Offshore Technology Conference*, OTC17733.

Ward, E.G. and Gebara, J.M. (2006), "Assessment of storm sea fastenings for drilling and workover rigs on floating production systems during hurricane ivan: phase 1", *Proceedings of Offshore Technology Conference,* OTC 18324.

Ward, E.G., Kim, M.H. and Bae, Y.H. (2010), "Tie-down loads for drilling rigs and modules on floating structures", *Proceedings of the OTC (Offshore Technology Conference) #20864*, Houston

Yang, C.K. (2009), *Numerical modeling of nonlinear coupling between lines/beams with multiple floating bodies*, Ph.D. Thesis, Texas A&M University.

Yang, Chan K., Bae, Y.H., Kim, M.H. and Ward, E.G. (2010a), "Loads on tie-down systems for floating drilling rigs during hurricane conditions", *J. ISOPE*.

Yang, Chan K. and Kim, M.H. (2010b), "Transient effects of tendon disconnection of a TLP by hull-tendon-riser coupled dynamic analysis", *Ocean Eng.*, **37**(8-9) , 667-677.

Yang, Chan K. and Kim, M.H. (2010c), "Linear and nonlinear approach of hydro-pneumatic tensioner modeling for spar global performance", *J. OMAE*, **132**(1).